Hindawi Publishing Corporation
International Journal of Polymer Science
Volume 2016, Article ID 1608939, 11 pages
http://dx.doi.org/10.1155/2016/1608939

Research Article

Competitive Fixed-Bed Adsorption of Pb(II), Cu(II), and Ni(II) from Aqueous Solution Using Chitosan-Coated Bentonite

Wan-Chi Tsai,[1] Mark Daniel G. de Luna,[2,3] Hanna Lee P. Bermillo-Arriesgado,[3] Cybelle M. Futalan,[4] James I. Colades,[3] and Meng-Wei Wan[5]

[1]*Department of Medical Laboratory Science and Biotechnology, Kaohsiung Medical University, Kaohsiung 80708, Taiwan*
[2]*Department of Chemical Engineering, University of the Philippines, Diliman, 1101 Quezon City, Philippines*
[3]*Environmental Engineering Program, National Graduate School of Engineering, University of Philippines, Diliman, 1101 Quezon City, Philippines*
[4]*Environment Business Line, Aecom Philippines Consultants Corporation, 1634 Taguig, Philippines*
[5]*Department of Environmental Resources Management, Chia Nan University of Pharmacy and Science, Tainan 71710, Taiwan*

Correspondence should be addressed to Meng-Wei Wan; peterwan@mail.cnu.edu.tw

Received 7 March 2016; Revised 6 May 2016; Accepted 25 May 2016

Academic Editor: Adel Mohamed

Fixed-bed adsorption studies using chitosan-coated bentonite (CCB) as adsorbent media were investigated for the simultaneous adsorption of Pb(II), Cu(II), and Ni(II) from a multimetal system. The effects of operational parameters such as bed height, flow rate, and initial concentration on the length of mass transfer zone, breakthrough time, exhaustion time, and adsorption capacity at breakthrough were evaluated. With increasing bed height and decreasing flow rate and initial concentration, the breakthrough and exhaustion time were observed to favorably increase. Moreover, the adsorption capacity at breakthrough was observed to increase with decreasing initial concentration and flow rate and increasing bed height. The maximum adsorption capacity at breakthrough of 13.49 mg/g for Pb(II), 12.14 mg/g for Cu(II), and 10.29 mg/g for Ni(II) was attained at an initial influent concentration of 200 mg/L, bed height of 2.0 cm, and flow rate of 0.4 mL/min. Adsorption data were fitted with Adams-Bohart, Thomas, and Yoon-Nelson models. Experimental breakthrough curves were observed to be in good agreement ($R^2 > 0.85$ and $E\% < 50\%$) with the predicted curves generated by the kinetic models. This study demonstrates the effectiveness of CCB in the removal of Pb(II), Cu(II), and Ni(II) from a ternary metal solution.

1. Introduction

The presence of heavy metals in groundwater and surface waters is considered a serious threat to the ecosystem and human health due to properties such as nonbiodegradability, bioaccumulation, and changing oxidation states [1]. Globally, the Philippines is ranked to be the fourth and fifth largest producer of Cu(II) and Ni(II), respectively. According to Republic Act 9275 (Philippine Clean Water Act of 2004), Pb(II) is generated during the ore mining and processing of Cu(II) and Ni(II) [2]. Based on the toxicological criteria, excessive intake of Pb(II) is considered to cause kidney damage, disruption of the nervous system, and delays in physical and mental development. Meanwhile, common metals such as Cu(II) and Ni(II) are considered to be essential minerals. However, ingestion of Cu(II) at high concentration may lead to central nervous system irritation, kidney failure, mucosal irritation, and liver damage while an increase in Ni(II) intake can cause health problems like lung, nose, and bone cancer as well as chronic bronchitis, respiratory distress, birth defects, and embolism [3–5]. Due to the deleterious effects of heavy metals on human health, the US Environmental Protection Agency has set a maximum contaminant level for Pb(II) and Cu(II) in drinking water to be at 0 mg/L and 1.3 mg/L, respectively.

Adsorption is a simple, highly effective, economically feasible, and environmentally benign technology utilized in the removal of heavy metals from industry effluents [6, 7].

In purification processes, liquid phase adsorption is typically carried out under varying configurations such as fixed-bed, fluidized bed, and batch. Fixed-bed adsorption has been proven to be an effective process under continuous flow conditions due to its operational simplicity, possibility of in situ generation, and ease of operation and handling [8, 9]. Moreover, only fixed-bed studies would provide readily available support data for the direct application of wastewater treatment in the industrial scale.

Chitosan-clay composites are considered to be a promising class of adsorbents due to their low production cost, improved materials, and mechanical stability [10]. Several studies using chitosan-coated montmorillonite composites were performed in the removal of tungsten [11], tannic acid [12], basic dyes [13, 14], humic acid [13], and reactive dyes [13]. L. Wang and A. Wang [10] investigated the adsorption of Congo red using *N*,*O*-carboxymethyl-chitosan/montmorillonite nanocomposites.

Chitosan-bentonite beads have been utilized in several studies for heavy metal removal, where the preparative method was similar to the process utilized by Wan et al. [15]. Basic comparative studies investigated the efficiency of removing Cu(II) from aqueous solution using chitosan-coated bentonite (CCB) cross-linked with epichlorohydrin, glutaraldehyde, and ethylene glycol diglycidyl ether [16, 17]. Other articles on CCB have been published, including removal of oxidized sulfur compounds [18], As(V) [19], In(III) [20], Pb(II) [2], Cu(II) [2], and Ni(II) [2]. Most of the previous studies on heavy metal removal using CCB were carried out in the batch mode. There were no reported fixed-bed studies on the competitive adsorption of Pb(II), Cu(II), and Ni(II) from multiple aqueous solutions. Moreover, it is essential to evaluate the simultaneous adsorption of two or more metals since single metal species rarely exist in wastewater effluents and natural waters [21–23]. In continuation of the previous work, this study aims to investigate the dynamics of the competitive adsorption of a multimetal system (Pb(II), Cu(II), and Ni(II)) using CCB under fixed-bed conditions. The effects of operational conditions such as bed height, solution flow rate, and initial ternary metal ion concentration on the shape of experimental breakthrough curves and corresponding equilibrium adsorption capacities were examined. The fixed-bed adsorption data were fitted to common dynamic models such as Adams-Bohart, Thomas, and Yoon-Nelson models and were evaluated using linear regression analysis. The validity of the kinetic models, in terms of accuracy and adequacy, was measured using error analysis.

2. Materials and Method

2.1. Chemicals. Chitosan powder with low molecular weight and 75–85% degree of deacetylation was procured from Sigma-Aldrich while bentonite was obtained from Riedel-de Haën. Lead nitrate ($Pb(NO_3)_2$), copper nitrate hemipentahydrate ($Cu(NO_3)_2{\cdot}2.5H_2O$), nickel nitrate hexahydrate ($Ni(NO_3)_2{\cdot}6H_2O$), sodium hydroxide (98% purity), hydrochloric acid (37% fuming), and inductively coupled plasma atomic emission spectroscopy (ICP-OES) multielement standard solutions were obtained from Merck (Germany).

2.2. Instrumentation. Infrared spectra of CCB before and after adsorption of Cu(II), Ni(II), and Pb(II) were obtained using a Nicolet 6700 Fourier Transform Infrared spectrometer using disc composed of 1 : 10 ratio of sample to KBr within the spectral range of 400–4000 cm^{-1}. The surface morphology and surface elemental analysis of CCB were observed by JEOL JSM-7001 scanning electron microscope (SEM) and energy dispersive X-ray spectroscopy (EDX) under a vacuum of 1.33×10^{-6} mBar, running at 20.0 kV and using a tungsten filament. The quantitative analysis for the residual concentration of metal ions was analyzed using ICP-OES Perkin Elmer DV2000 series.

2.3. Synthesis of Chitosan-Coated Bentonite. Based on the method by Wan et al. [15], CCB beads were synthesized by dissolving 5.0 g chitosan in 5% (v/v) HCl (300 mL) where the mixture was stirred for 2 h at 300 rpm. About 100 g of bentonite was slowly added to the solution and stirred for another 3 h. Sodium hydroxide (1 N) was added dropwise until neutral pH was obtained. The resulting beads were thoroughly washed with deionized water and dried in an oven (Chanel Precision Oven DV452, Memmert GmbH) for 24 h at 65°C. Then, the CCB beads were pulverized and sieved where particles with size range of 0.50 to 0.21 mm were used in the fixed-bed studies.

2.4. Fixed-Bed Experiments. The schematic diagram of the fixed-bed adsorption set-up is shown in Figure 1. Fixed-bed adsorption experiments were carried out using a 1.8 cm i.d., 76 cm length borosilicate glass column (7740, IWAKI). Near the column inlet, glass beads and sand were placed to prevent channeling and ensure even distribution of the solution. Glass wool and sand were placed at the bottom to prevent loss of the CCB and avoid outlet clogging. The fixed-bed was continuously operated in a down flow mode using a peristaltic pump (Model 7518-00, Cole Palmer) at room temperature (25 ± 1°C). The pH of the influent was maintained at a constant pH 4.0 [17]. Effluent samples were collected from the bottom of the fixed-bed at predetermined time intervals. Operating parameters such as initial concentration (50–200 mg/L), flow rate (0.6–1.0 mL/min), and bed height (1.0–3.0 cm) were varied.

2.5. Analysis of the Breakthrough Curves. The column performance in the removal of Pb(II), Ni(II), and Cu(II) from a multimetal system is analyzed using breakthrough curves. The breakthrough time is described as the time when the effluent metal concentration is about 3–5% of the influent concentration [24]. In this study, the breakthrough time (t_b, min) is set as the time when the effluent metal concentration reaches 1% of the influent concentration while exhaustion time (t_{total}, min) is set as the time when the concentration of the effluent becomes constant and breakthrough curves become flat.

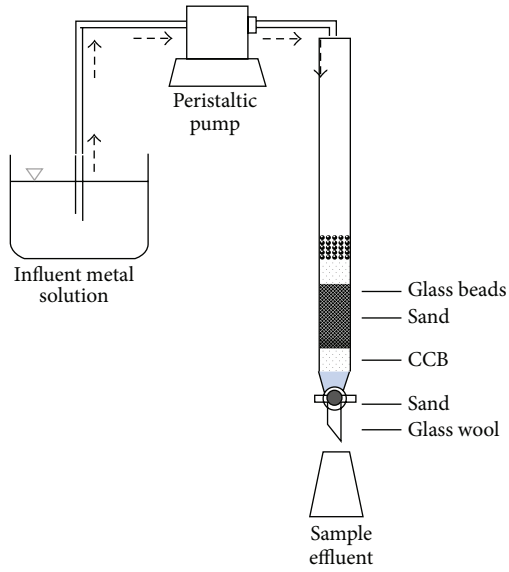

Figure 1: Fixed-bed adsorption set-up for multimetal adsorption unto CCB.

The total adsorbed metal quantity (q, mg) in the column is represented by the area under the plot of the adsorbed metal ion concentration, which is calculated through numerical integration, given as

$$q = \frac{QA}{1000} = \frac{Q}{1000}\int_0^t (C_0 - C_t)\,dt, \tag{1}$$

where Q corresponds to the solution flow rate (mL/min), C_0 is the influent concentration (mg/L), C_t is the effluent concentration (mg/L) at any time t (min), and A refers to the area under the breakthrough curve from C_0 to C_t (mg·min/L) from time 0 to any time t [24].

The total metal uptake at equilibrium, q_e (mg/g), is computed using

$$q_e = \frac{q}{m}, \tag{2}$$

where m (g) corresponds to the mass of adsorbent [24]. The total equilibrium adsorption capacity, q_{total} (mg/g), for n number of components is calculated using

$$q_{\text{total}} = \frac{\sum_{i=1}^{n} q_{(i)}}{m}. \tag{3}$$

The length of the mass transfer zone, MTZ (cm), is dependent on the bed height, L (cm), and breakthrough and equilibrium point as computed in [25]

$$\text{MTZ} = \left(\frac{t_{\text{total}} - t_b}{t_{\text{total}}}\right) L. \tag{4}$$

The volume of effluent treated, V_{eff} (mL), is calculated using

$$V_{\text{eff}} = Qt_{\text{total}}. \tag{5}$$

2.6. Error Analysis. Error analysis is performed in order to validate the most applicable model that would describe the performance of the breakthrough curves in the fixed-bed adsorption of a multimetal system using CCB. In general, the fit between experimental data and linearized forms could be illustrated using the linear regression correlation coefficient (R^2). On the other hand, the average percentage error (E%) describes the agreement between the theoretical and experimental values of C_t/C_0 that was utilized in plotting breakthrough curves [26]. Values of E% that are <35% are considered to be acceptable [27]:

$$E\% = \frac{\sum_{i=1}^{N}\left[\left|(C_t/C_0)_{\text{exp}} - (C_t/C_0)_{\text{theo}}\right| / (C_t/C_0)_{\text{exp}}\right]}{N} \times 100. \tag{6}$$

3. Results and Discussion

3.1. FTIR Analysis. The FTIR spectra of CCB before and after adsorption of Pb(II), Cu(II), and Ni(II) were presented in Figure 2. There are several characteristic peaks that can be attributed to chitosan such as 3442 cm^{-1} due to hydroxyl O-H stretching vibration and extension vibration of N-H; 3656 due to O-H stretching of the alcohol group; 1638 due to the stretching vibrations of amide carbonyl groups C=O; and 1383 cm^{-1} due to the bending vibration of methylene group CH_2= [28, 29]. The remaining predominant peaks, namely, 1048 cm^{-1} due to Si-O-Si stretching; 919 cm^{-1} due to Al-OH stretching; 798 cm^{-1} due to (Al, Mg)-OH stretching; 526 cm^{-1} due to Si-O-Al bending; and 466 cm^{-1} due to Si-O-Si bending, are characteristic bands of bentonite [14]. Based on Table 1, the apparent shift in transmittance from 3656, 3442, 1048, and 466 cm^{-1} to 3662, 3451, 1056, and 473 cm^{-1} confirmed that the hydroxyl and amine groups of chitosan as well as Si-O groups of bentonite were involved in the adsorption of Pb(II), Cu(II), and Ni(II).

3.2. SEM-EDX Analysis. Figures 3 and 4 present the SEM micrographs and EDX spectra of unused CCB and CCB loaded with Pb(II), Cu(II), and Ni(II), respectively. The surface morphology of CCB before metal adsorption was observed to be irregular and coarse. After metal adsorption, the CCB surface becomes more agglomerated and packed. Based on Figure 4, the presence of aluminum, magnesium, and silicon peaks is attributed to bentonite [14] while carbon and oxygen peaks are assigned to chitosan. After adsorption, CCB beads loaded with metals were shown to have the following elements: Al (9.90%), C (3.45%), Mg (1.65%), O (54.54%), and Si (27.89%) with additional peaks such as Pb(II) (1.25%), Cu(II) (0.87%), and Ni(II) (0.45%) were observed to be present.

3.3. Effect of Flow Rate. The effect of flow rate (0.6 to 1.0 mL/min) on the fixed-bed removal of Pb(II), Cu(II), and Ni(II) was evaluated while the bed depth and initial concentration were maintained at 2.0 cm and 100 mg/L, respectively. Based on Figure 5, the breakthrough curves

Table 1: FTIR analysis of CCB (before and after adsorption).

IR peak	Wavenumber (cm^{-1})			Assignment
	Before adsorption	After adsorption	Differences	
1	3442	3451	+9	O-H stretching
2	3656	3662	+6	N-H stretching
3	1638	1638	0	C=O stretching
4	1383	1383	0	CH_2= bending
5	1048	1056	+8	Si-O-Si stretching
6	920	920	0	Al-OH stretching
7	798	798	0	(Al, Mg)-OH stretching
8	526	526	0	Si-O-Al bending
9	466	473	+7	Si-O-Si bending

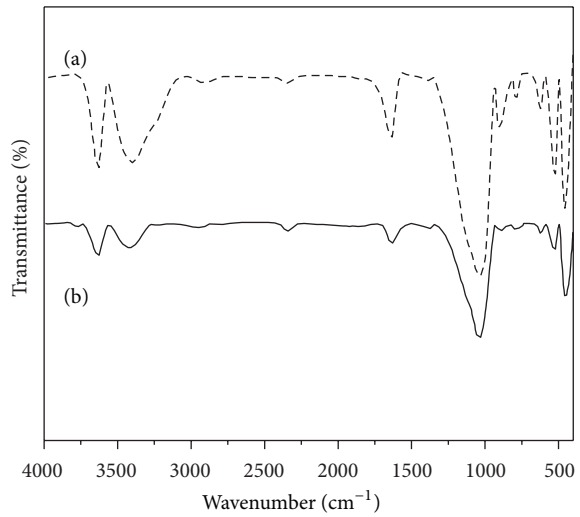

Figure 2: FTIR spectra of (a) CCB before adsorption and (b) CCB after adsorption.

were observed to shift from right to left with increasing flow rate, which indicates shorter service time of the bed. Unlike the steeper and more defined breakthrough curves of 0.8 and 1.0 mL/min, those of 0.6 mL/min are characterized by a gradual slope (lower value of dC/dt). In Table 2, an increase in flow rate resulted in lower breakthrough and exhaustion times as well as longer mass transfer zones. This is due to decrease in residence time and higher intraparticle diffusion effect of the aqueous solution in the fixed-bed at higher flow rates [30]. In addition, the total volume of effluent treated (V_{eff}) and quantity of metal ions adsorbed at exhaustion (q_e) were observed to also decrease at higher flow rates. The reduced contact time at greater flow rates indicates that there is less time for lateral diffusion to occur within the CCB bed due to weak distribution of the liquid inside the fixed-bed, which results in lower diffusivity of the solute among the adsorbent particles [31–33].

3.4. Effect of Bed Height. As seen in Figure 6, the breakthrough curves of Pb(II), Cu(II), and Ni(II) become less steep as bed depth was increased from 1.0 to 3.0 cm. Moreover, as the bed height was increased, breakthrough curves were observed to shift from left to right that resulted in longer times to reach breakthrough and exhaustion (Table 3). It can also be seen that the increasing adsorbent bed height prolonged the breakthrough time (t_b) and exhaustion time (t_{total}) as well as a significant increase in volume of treated effluent (V_{eff}) of the fixed-bed. The increase in the removal of Pb(II), Cu(II), and Ni(II) can be attributed to greater amount of CCB present in the fixed-bed at 2.0 and 3.0 cm, which implies that there are more binding sites available that would result in higher breakthrough adsorption capacity of the column [34]. The good performance of metal removal at bed height of 3.0 cm could also be attributed to more contact opportunities between the metal and CCB particles. However, the mass transfer zone broadened since an increase in bed height causes greater resistance to mass transfer and slower kinetics of adsorption [35]. The increased mass transfer resistance is caused by the repulsive forces between the adsorbed metals on the CCB's surface and metals in the aqueous film.

3.5. Effect of Influent Concentration. The breakthrough curves of Pb(II), Cu(II), and Ni(II) under varying influent concentration are shown in Figure 7. When the ternary influent concentration was increased from 50 to 200 mg/L, steeper and sharper breakthrough curves were obtained with higher values of dC/dt at 150 and 200 mg/L. In Table 4, results show that the fixed-bed was saturated more quickly, where earlier breakthrough time and exhaustion time were achieved at high metal concentration (200 mg/L). As a result, the total volume of effluent treated (V_{eff}) decreased. However, adsorption capacity at equilibrium (q_e) was observed to increase at high influent concentration. In adsorption, the main driving force is the concentration gradient, which is the difference between the concentration of solute on the sorbent and concentration of solute in the solution [36]. At higher metal concentration, the driving force of adsorption is greater due to the high concentration difference facilitated by high mass transfer coefficient values. Thus, higher adsorption capacities are achieved at higher metal concentration. The values of MTZ were observed to decrease with increase in influent metal concentration.

Table 2: Column adsorption data and parameters of ternary metal solution of Pb(II), Cu(II), and Ni(II) at different solution flow rates with initial metal concentration of 100 mg/L and bed height of 2.0 cm.

Q (mL/min)	Metal	dC/dt (mg/L·h)	t_b (min)	t_{total} (min)	V_{eff} (mL)	MTZ (cm)	q_e (mg/g)	q_{total} (mg/g)
0.6	Pb(II)	0.18	260.34	660	396	1.21	11.35	24.55
	Cu(II)	0.21	217.10	540	324	1.20	8.90	
	Ni(II)	0.24	165.27	480	288	1.31	8.13	
0.8	Pb(II)	0.27	147.46	450	360	1.34	9.43	23.44
	Cu(II)	0.28	124.97	420	336	1.41	7.75	
	Ni(II)	0.30	95.38	390	312	1.51	6.26	
1.0	Pb(II)	0.33	123.03	390	390	1.37	9.96	23.46
	Cu(II)	0.31	99.70	390	390	1.49	7.71	
	Ni(II)	0.37	74.60	330	330	1.55	5.79	

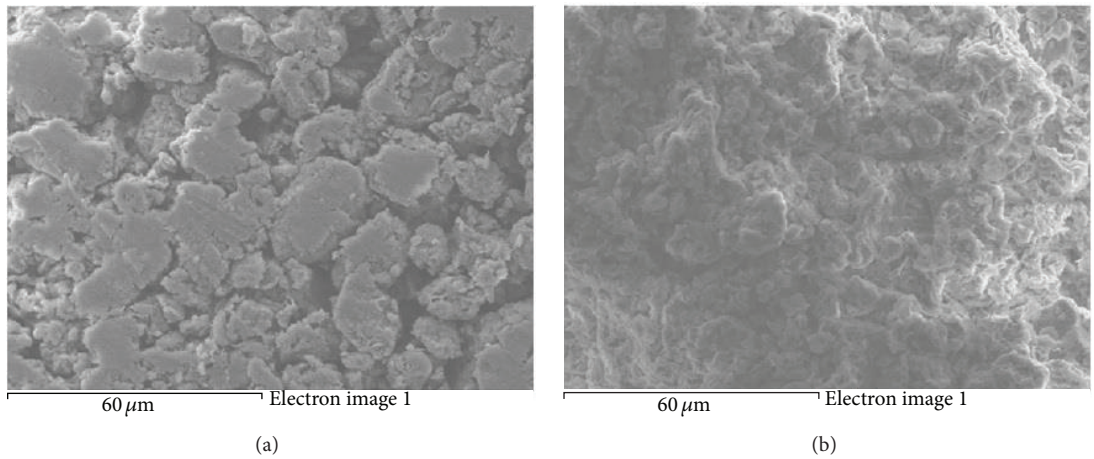

(a) (b)

Figure 3: SEM micrographs of (a) CCB before adsorption and (b) CCB after adsorption.

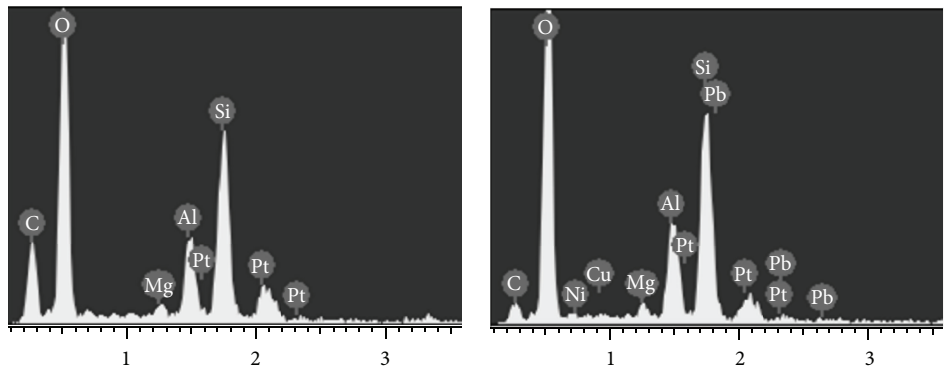

(a) (b)

Figure 4: EDX spectra of unused CCB (a) and CCB after adsorption of Pb(II), Cu(II), and Ni(II) (b).

3.6. Application of Mathematical Kinetic Model. Fixed-bed adsorption data was fitted with established mathematical models in order to predict breakthrough curves and to subsequently determine the model parameters. The modeling of the breakthrough curves utilized experimental data with C_t/C_0 values higher than 0.01 to less than 0.99 using Adams-Bohart, Thomas, and Yoon-Nelson kinetic models.

The Thomas model evaluates the maximum solid phase concentration of solute on the adsorbent and the rate constant in a fixed-bed [27]. The model is based on the following

Table 3: Column adsorption data and parameters of ternary metal solution of Pb(II), Cu(II), and Ni(II) at different bed heights with initial metal concentration of 100 mg/L and flow rate of 0.6 mL/min.

L (cm)	Metal	dC/dt (mg/L·hr)	t_b (min)	t_{total} (min)	V_{eff} (mL)	MTZ (cm)	q_e (mg/g)	q_{total} (mg/g)
1.0	Pb(II)	0.20	117.58	540	216	0.78	9.47	24.58
	Cu(II)	0.22	98.57	480	192	0.79	8.10	
	Ni(II)	0.22	77.19	480	192	0.84	7.01	
2.0	Pb(II)	0.13	338.19	870	348	1.22	10.65	26.67
	Cu(II)	0.15	273.76	780	312	1.30	8.70	
	Ni(II)	0.19	202.83	630	252	1.36	7.32	
3.0	Pb(II)	0.07	406.68	1560	624	2.22	11.47	28.13
	Cu(II)	0.07	344.07	1440	576	2.30	8.76	
	Ni(II)	0.08	283.23	1380	552	2.30	7.91	

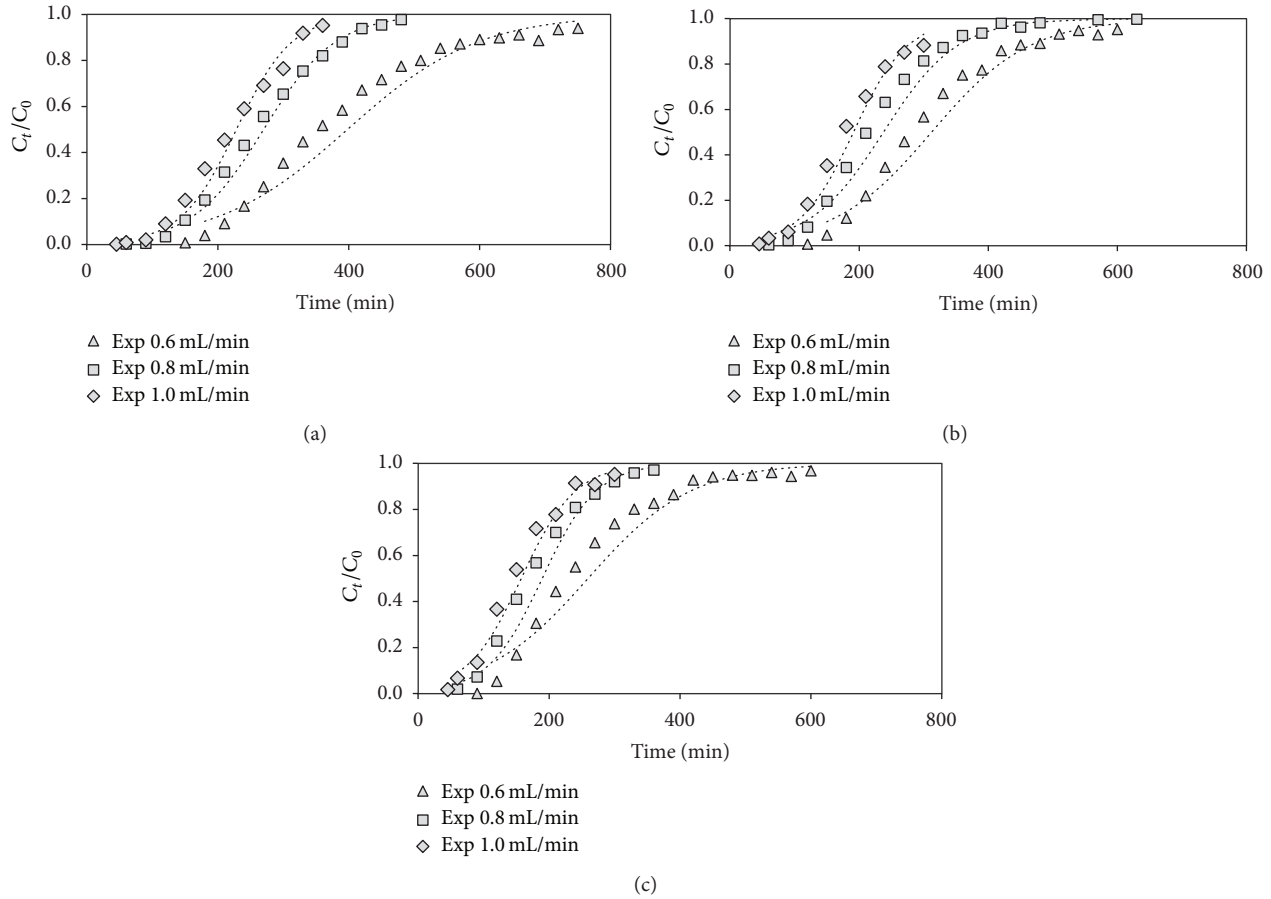

Figure 5: Experimental breakthrough curves at different flow rates of ternary metal solution of (a) Pb(II), (b) Cu(II), and (c) Ni(II) (C_0 = 100 mg/L; Q = 0.4 mL/min; model fit is shown as ⋯).

assumptions: negligible axial and radial dispersion in the fixed-bed; adsorption that follows Langmuir isotherm of adsorption-desorption; and the rate driving force obeying second-order reversible reaction kinetics [37]. The linearized form of the Thomas model is expressed as

$$\ln\left(\frac{C_0}{C_t} - 1\right) = \frac{k_{\text{TH}} q_e m}{Q} - k_{\text{TH}} C_0 t, \tag{7}$$

where k_{TH} is the Thomas rate constant (mL/min·mg); q_e is the adsorption capacity at equilibrium (mg/g); m is the amount of adsorbent in the column (g); and Q is the solution flow rate (mL/min) [38].

The Adams-Bohart model is an analytical expression based on the assumption of a rectangular isotherm, where the adsorption rate is proportional to both the residual capacity of the sorbent and adsorbate concentration [39, 40]. The linearized Adams-Bohart equation is provided as

$$\ln\left(\frac{C_0}{C_t} - 1\right) = k_{\text{AB}} N_o \frac{Z}{F} - k_{\text{AB}} C_0 t, \tag{8}$$

Table 4: Column adsorption data of ternary metal solution of Pb(II), Cu(II), and Ni(II) at different initial metal concentration with bed height of 2.0 cm and solution flow rate of 0.4 mL/min.

C_0 (mg/L)	Metal	dC/dt (mg/L·hr)	t_b (min)	t_{total} (min)	V_{eff} (mL)	MTZ (cm)	q_e (mg/g)	q_{total} (mg/g)
50	Pb(II)	0.03	794.57	2040	816	1.11	11.53	30.74
	Cu(II)	0.03	618.91	2040	816	1.15	10.12	
	Ni(II)	0.03	482.58	1860	744	1.36	9.09	
150	Pb(II)	0.28	322.94	780	312	1.17	14.31	34.90
	Cu(II)	0.29	325.07	720	288	1.10	10.84	
	Ni(II)	0.32	221.06	630	252	1.30	9.75	
200	Pb(II)	0.51	268.21	600	240	1.22	13.49	35.92
	Cu(II)	0.53	243.52	570	228	1.34	12.14	
	Ni(II)	0.50	172.30	540	216	1.48	10.29	

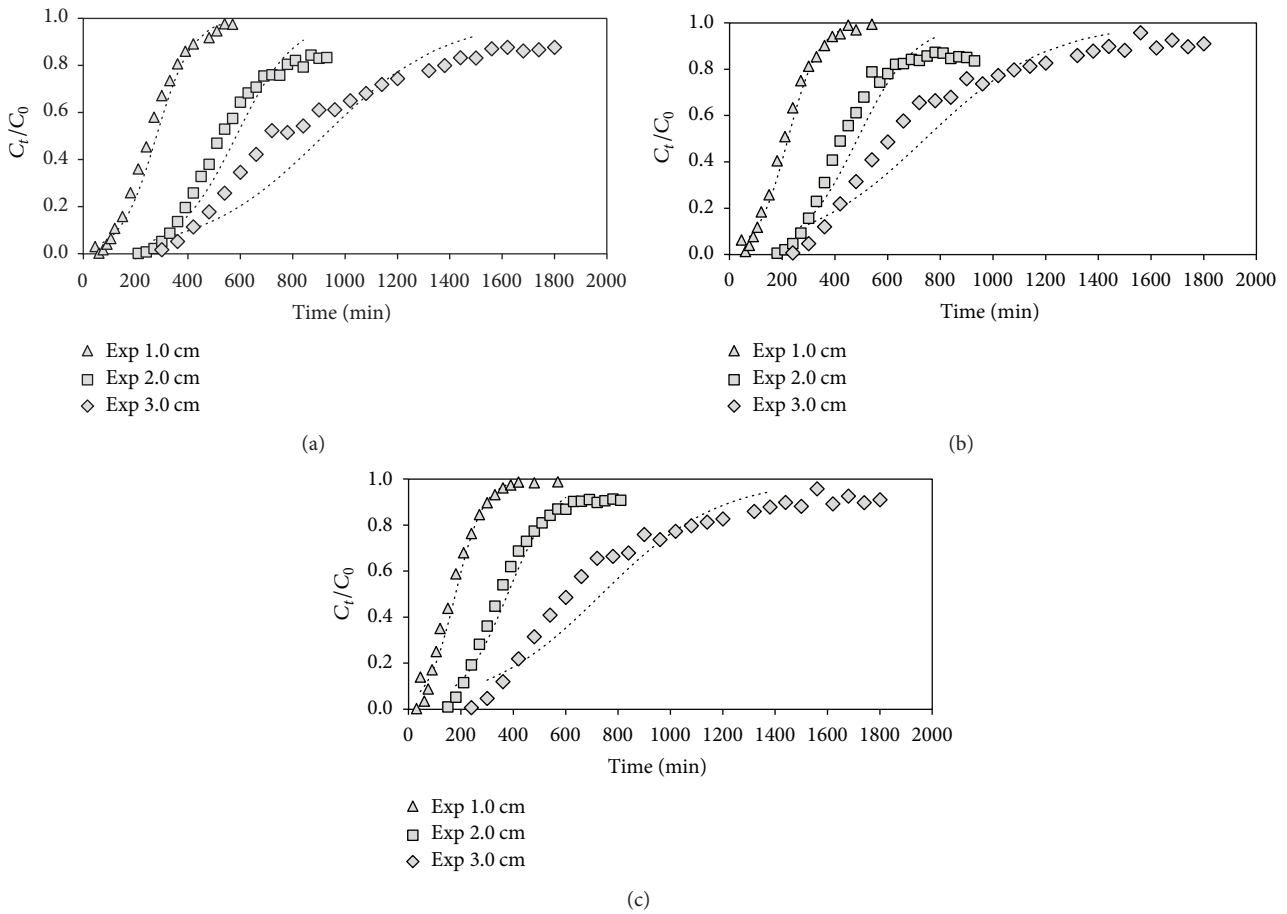

Figure 6: Experimental breakthrough curves at different bed heights of ternary metal solution of (a) Pb(II), (b) Cu(II), and (c) Ni(II) (C_0 = 100 mg/L; Q = 0.4 mL/min; model fit is shown as ⋯).

where k_{AB} is the Adams-Bohart kinetic rate constant (L/mg·min); N_o is the saturation concentration of the adsorbent (mg/L); Z is the bed height of the adsorbent (cm); F is the linear flow rate (cm/min).

The Yoon-Nelson model assumes that the rate of decrease in the probability of the adsorbate molecule being adsorbed is proportional to the probability of the adsorbate adsorption and adsorbate breakthrough on the adsorbent [31, 41]. It is expressed by

$$\ln\left(\frac{C_0}{C_t} - 1\right) = \tau k_{YN} - k_{YN} t, \tag{9}$$

where τ is the time required for 50% adsorbate breakthrough (min) and k_{YN} is the Yoon-Nelson rate constant (L/min).

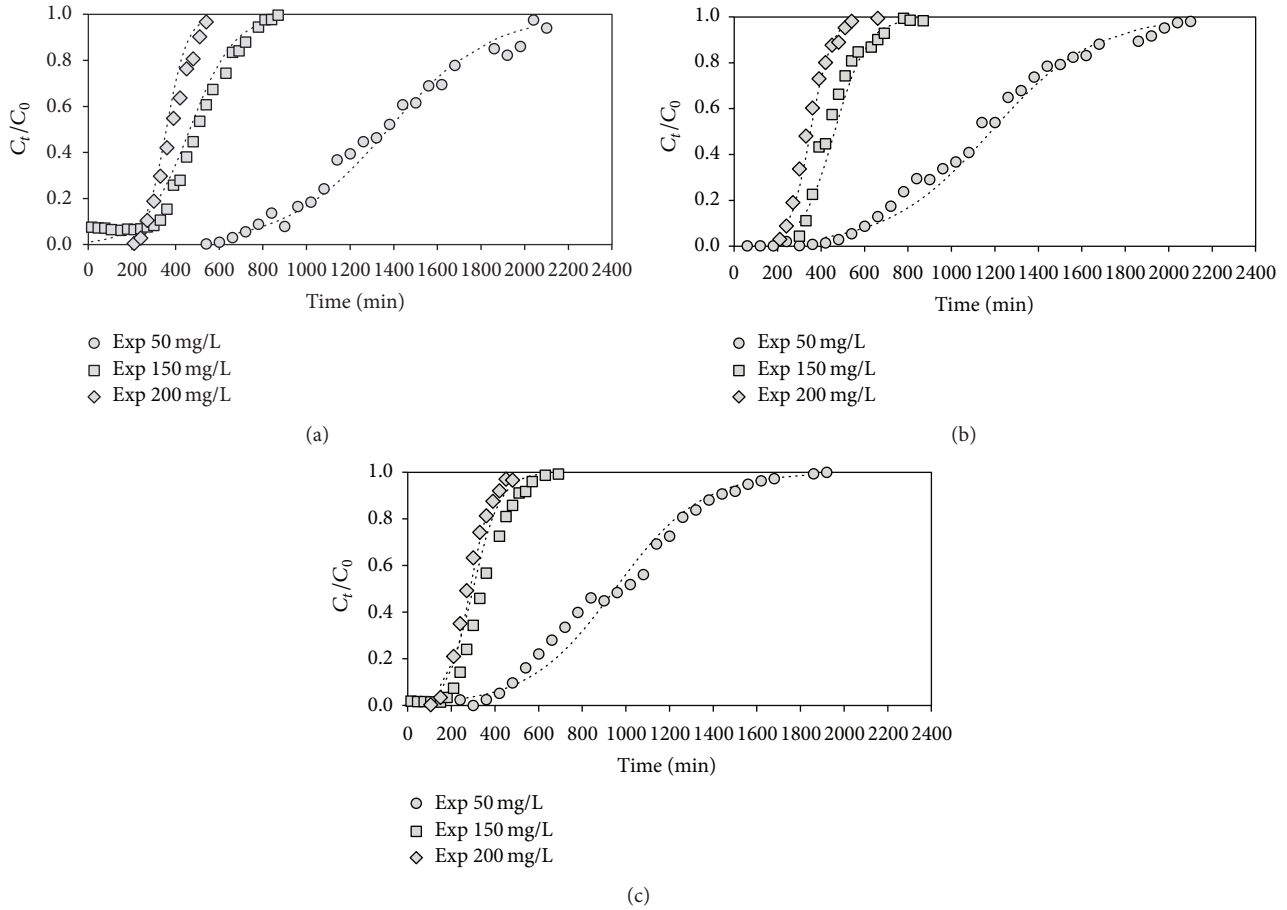

Figure 7: Experimental breakthrough curves at different initial concentration of ternary metal solution of (a) Pb(II), (b) Cu(II), and (c) Ni(II) (L = 2.0 cm; Q = 0.4 mL/min; model fit is shown as $\cdots$).

All three kinetic models are considered to be mathematically equivalent, which can be represented by a similar fitting equation:

$$\ln\left[\frac{C_0}{C_t} - 1\right] = a - bt, \tag{10}$$

where a represents $k_{TH}q_e m/Q$ (Thomas model), $k_{AB}N_o Z/F$ (Adams-Bohart model), and τk_{YN} (Yoon-Nelson model), while b is equivalent to $k_{TH}C_0$ (Thomas model), $k_{AB}C_0$ (Adams-Bohart model), and k_{YN} (Yoon-Nelson model).

The values of the model parameters derived from Adams-Bohart, Thomas, and Yoon-Nelson are presented in Table 5. Based on the high R^2 values ($0.85 < R^2 < 0.99$) and low values of E%, all three kinetic models (Adams-Bohart, Thomas, and Yoon-Nelson) best describe the simultaneous fixed-bed adsorption of Pb(II), Cu(II), and Ni(II) from a multimetal system.

As the flow rate was increased, all kinetic coefficients of the three models (k_{AB}, k_{TH}, and k_{YN}) were observed to increase while N_o, q_e, and τ decreased. This implies that external mass transfer dominates the fixed-bed kinetics that occurs at the initial part of the adsorption [31]. Moreover, the values of the rate constant are determined by the mass transfer in the fluid that is dependent on the flow rate [42].

Based on Table 5, increasing the bed height from 1.0 to 3.0 cm causes the values of kinetic rate constants (k_{AB}, k_{TH}, k_{YN}) and q_e, N_o, and τ to increase. A longer bed height translates to longer contact time of the solution through the fixed-bed. Moreover, a lower rate constant indicates there is sufficient time for the contaminants to migrate from bulk solution to be adsorbed onto CCB surface.

At higher influent concentration, the adsorption bed capacity (N_o) and adsorption capacity at equilibrium (q_e) were observed to increase while 50% time to reach breakthrough (τ) decreased. However, there was no apparent trend observed for k_{AB} and k_{TH} while values of k_{YN} significantly increased with increasing influent concentration. The increase in k_{YN} was due to the increase in driving force of mass transfer in liquid film which leads to easy saturation of the fixed-bed and resulted in a decrease in t_{50} [43]. Based on Figures 5–7, the predicted breakthrough curves are in good agreement with the experimental data, which implies that models such as Adams-Bohart, Yoon-Nelson, and Thomas are adequate in predicting the fixed-bed adsorption behavior of Pb(II), Cu(II), and Ni(II) in a multimetal system.

3.7. Selectivity of CCB in the Removal of Pb(II), Cu(II), and Ni(II). In all experimental runs, Pb(II) was observed

Table 5: Model parameters of Adams-Bohart, Thomas, and Yoon-Nelson equation for the fixed-bed adsorption of Pb(II), Cu(II), and Ni(II) onto CCB at 25°C.

	Column conditions			Adams-Bohart model				Thomas model					Yoon-Nelson model				
Metal	L (cm)	C_0 (mg/L)	Q (mL/min)	N_o (mg/L)	k_{AB} $\times 10^{-4}$ (L/mg·min)	R^2	E%	$q_{e(theo)}$ (mg/g)	$q_{e(exp)}$ (mg/g)	k_{TH} $\times 10^{-4}$ (L/mg·min)	R^2	E%	$\tau_{(theo)}$ (min)	$\tau_{(exp)}$ (min)	k_{YN} $\times 10^{-2}$ (L/min)	R^2	E%
	1.0	100	0.4	4209.67	1.54	0.96	22.39	10.69	9.47	1.48	0.96	24.57	279.22	251.04	1.42	0.96	24.57
Pb	2.0	100	0.4	4431.50	0.92	0.91	22.97	11.30	10.65	0.84	0.91	26.43	585.73	525.52	0.81	0.91	26.43
	3.0	100	0.4	4911.13	0.42	0.85	32.71	12.50	11.47	0.36	0.85	40.61	917.62	706.63	0.37	0.85	40.61
	1.0	100	0.4	3377.24	1.76	0.97	13.72	8.56	8.10	1.71	0.97	14.44	221.07	207.51	1.66	0.97	14.44
Cu	2.0	100	0.4	3695.78	0.95	0.87	22.49	9.29	8.70	0.83	0.87	25.67	480.61	424.49	0.80	0.87	25.67
	3.0	100	0.4	3702.29	0.45	0.86	23.07	9.21	8.76	0.39	0.86	27.28	727.19	609.80	0.37	0.86	27.28
	1.0	100	0.4	2804.52	1.87	0.97	23.15	7.10	7.01	1.81	0.97	23.97	178.49	162.47	1.80	0.97	23.97
Ni	2.0	100	0.4	3057.98	1.07	0.95	14.83	7.75	7.32	1.01	0.95	15.91	377.05	347.00	1.04	0.95	15.91
	3.0	100	0.4	4013.31	0.43	0.88	22.16	10.02	7.91	0.38	0.88	25.39	723.79	487.28	0.39	0.88	25.39
	2.0	50	0.4	4508.82	1.03	0.95	13.06	11.50	11.53	0.98	0.95	13.62	1377.80	1357.50	0.41	0.95	13.62
Pb	2.0	150	0.4	5447.87	0.65	0.91	33.73	13.96	14.31	0.60	0.91	34.70	468.59	498.09	0.89	0.91	34.70
	2.0	200	0.4	5560.37	1.12	0.98	15.74	14.15	13.49	1.09	0.98	15.79	387.38	378.75	1.99	0.98	15.79
	2.0	50	0.4	4041.36	0.97	0.96	19.54	10.28	10.12	0.93	0.96	20.80	1181.82	1122.01	0.41	0.96	20.80
Cu	2.0	150	0.4	4643.90	1.04	0.93	19.36	11.66	10.84	0.97	0.93	22.28	456.44	432.61	1.23	0.93	22.28
	2.0	200	0.4	5145.37	1.11	0.98	13.08	13.07	12.14	1.08	0.98	13.94	350.90	334.93	2.02	0.98	13.94
	2.0	50	0.4	3496.66	1.08	0.98	14.90	8.88	9.09	1.05	0.98	15.29	948.80	986.39	0.49	0.98	15.29
Ni	2.0	150	0.4	3424.99	1.09	0.87	18.90	8.32	9.75	0.94	0.87	26.30	285.91	310.81	1.37	0.87	13.74
	2.0	200	0.4	4411.13	1.03	0.98	13.21	11.18	10.29	1.00	0.98	13.74	285.02	272.84	1.96	0.98	13.74
	2.0	100	0.6	4393.32	1.07	0.92	18.59	11.03	11.35	0.99	0.92	21.80	392.63	414.24	0.93	0.92	21.80
Pb	2.0	100	0.8	4260.21	1.94	0.99	11.98	10.15	9.43	1.91	0.99	11.93	269.77	256.58	1.79	0.99	11.93
	2.0	100	1.0	3995.00	2.47	0.97	18.97	10.85	9.96	2.40	0.97	19.43	228.40	220.18	2.28	0.97	19.43
	2.0	100	0.6	3283.42	1.48	0.94	16.58	8.24	8.90	1.39	0.94	19.12	308.08	331.56	1.24	0.94	19.12
Cu	2.0	100	0.8	3463.43	1.89	0.96	22.13	8.69	7.75	1.82	0.96	24.88	234.15	211.16	1.68	0.96	24.88
	2.0	100	1.0	3405.03	2.64	0.97	14.78	8.68	7.71	2.57	0.97	16.39	191.36	175.50	2.33	0.97	16.39
	2.0	100	0.6	2970.38	1.31	0.91	18.55	7.27	8.13	1.19	0.91	22.22	249.64	274.35	1.16	0.91	22.22
Ni	2.0	100	0.8	2843.00	2.52	0.96	21.72	7.20	6.26	2.43	0.96	24.58	188.60	167.13	2.32	0.96	24.58
	2.0	100	1.0	3013.23	2.47	0.97	12.40	7.63	5.79	2.38	0.97	14.10	156.49	143.27	2.33	0.97	14.10

to be preferentially adsorbed over Cu(II) and Ni(II) in a multimetal system. Breakthrough and exhaustion of the fixed-bed occurred earlier for Ni(II) over Cu(II) and Pb(II). As such, the total amount of metal ions adsorbed by the column (q_{ad}) was in the order of Pb(II) > Cu(II) > Ni(II). The selectivity can be attributed to the difference in metal properties such as electronegativity and hydrolysis constant, with Pb(II) being the most electronegative and being easily hydrolyzed in comparison to Cu(II) and Ni(II) [44]. Thus, more Pb(II) was adsorbed by the functional groups of CCB. Previous batch studies showed similar results, where Pb(II) has the greatest affinity for adsorption onto CCB over Cu(II) and Ni(II) [2].

4. Conclusion

The performance of CCB in removing Pb(II), Cu(II), and Ni(II) from multimetal solution under fixed-bed conditions was evaluated. Breakthrough curves were derived under varying flow rate, bed height, and initial metal concentration. Results indicate that the breakthrough time, exhaustion time, and adsorption capacity at breakthrough increase with decreasing flow rate and initial concentration and increasing bed height. The adsorption preference of CCB could be arranged in the order of Pb(II) > Cu(II) > Ni(II). Experimental breakthrough curves were observed to be in good agreement with theoretical curves generated by Adams-Bohart, Thomas, and Yoon-Nelson models, which were validated by high R^2 ($R^2 > 0.85$) and low E% values (E% < 35%). FTIR analysis showed that hydroxyl (O-H) and amine (N-H) groups of chitosan and Si-O group of bentonite are involved in the adsorption process. This study demonstrates that CCB is an effective adsorbent in the removal of Pb(II), Cu(II), and Ni(II) from a multimetal solution.

Competing Interests

The authors declare that they have no competing interests.

Acknowledgments

This research was financially supported by the Taiwan National Science Council (NSC 97-2221-E-041-016), Military of Science Technology (MOST 104-2221-E-041-002), and the Department of Science and Technology, Philippines, through the Engineering Research and Development for Technology (ERDT).

References

[1] W. S. Wan Ngah, A. Kamari, and Y. J. Koay, "Equilibrium and kinetics studies of adsorption of copper (II) on chitosan and chitosan/PVA beads," *International Journal of Biological Macromolecules*, vol. 34, no. 3, pp. 155–161, 2004.

[2] C. M. Futalan, C.-C. Kan, M. L. Dalida, K.-J. Hsien, C. Pascua, and M.-W. Wan, "Comparative and competitive adsorption of copper, lead, and nickel using chitosan immobilized on bentonite," *Carbohydrate Polymers*, vol. 83, no. 2, pp. 528–536, 2011.

[3] M. Liu, Y. Deng, H. Zhan, and X. Zhang, "Adsorption and desorption of copper(II) from solutions on new spherical cellulose adsorbent," *Journal of Applied Polymer Science*, vol. 84, no. 3, pp. 478–485, 2002.

[4] R. Han, L. Zou, X. Zhao et al., "Characterization and properties of iron oxide-coated zeolite as adsorbent for removal of copper(II) from solution in fixed bed column," *Chemical Engineering Journal*, vol. 149, no. 1–3, pp. 123–131, 2009.

[5] A. Rahmani, H. Z. Mousavi, and M. Fazli, "Effect of nanostructure alumina on adsorption of heavy metals," *Desalination*, vol. 253, no. 1–3, pp. 94–100, 2010.

[6] K. Swayampakula, V. M. Boddu, S. K. Nadavala, and K. Abburi, "Competitive adsorption of Cu (II), Co (II) and Ni (II) from their binary and tertiary aqueous solutions using chitosan-coated perlite beads as biosorbent," *Journal of Hazardous Materials*, vol. 170, no. 2-3, pp. 680–689, 2009.

[7] U. Kumar and M. Bandyopadhyay, "Fixed bed column study for Cd(II) removal from wastewater using treated rice husk," *Journal of Hazardous Materials*, vol. 129, no. 1–3, pp. 253–259, 2006.

[8] K. Z. Setshedi, M. Bhaumik, M. S. Onyango, and A. Maity, "Breakthrough studies for Cr(VI) sorption from aqueous solution using exfoliated polypyrrole-organically modified montmorillonite clay nanocomposite," *Journal of Industrial and Engineering Chemistry*, vol. 20, no. 4, pp. 2208–2216, 2014.

[9] S. Kundu and A. K. Gupta, "Analysis and modeling of fixed bed column operations on As(V) removal by adsorption onto iron oxide-coated cement (IOCC)," *Journal of Colloid and Interface Science*, vol. 290, no. 1, pp. 52–60, 2005.

[10] L. Wang and A. Wang, "Adsorption behaviors of Congo red on the *N,O*-carboxymethyl-chitosan/montmorillonite nanocomposite," *Chemical Engineering Journal*, vol. 143, no. 1–3, pp. 43–50, 2008.

[11] H. Gecol, P. Miakatsindila, E. Ergican, and S. R. Hiibel, "Biopolymer coated clay particles for the adsorption of tungsten from water," *Desalination*, vol. 197, no. 1–3, pp. 165–178, 2006.

[12] J.-H. An and S. Dultz, "Adsorption of tannic acid on chitosan-montmorillonite as a function of pH and surface charge properties," *Applied Clay Science*, vol. 36, no. 4, pp. 256–264, 2007.

[13] M.-Y. Chang and R.-S. Juang, "Adsorption of tannic acid, humic acid, and dyes from water using the composite of chitosan and activated clay," *Journal of Colloid and Interface Science*, vol. 278, no. 1, pp. 18–25, 2004.

[14] P. Monvisade and P. Siriphannon, "Chitosan intercalated montmorillonite: preparation, characterization and cationic dye adsorption," *Applied Clay Science*, vol. 42, no. 3-4, pp. 427–431, 2009.

[15] M.-W. Wan, I. G. Petrisor, H.-T. Lai, D. Kim, and T. F. Yen, "Copper adsorption through chitosan immobilized on sand to demonstrate the feasibility for in situ soil decontamination," *Carbohydrate Polymers*, vol. 55, no. 3, pp. 249–254, 2004.

[16] N. Grisdanurak, S. Akewaranugulsiri, C. M. Futalan et al., "The study of copper adsorption from aqueous solution using crosslinked chitosan immobilized on bentonite," *Journal of Applied Polymer Science*, vol. 125, no. 2, pp. E132–E142, 2012.

[17] M. L. P. Dalida, A. F. V. Mariano, C. M. Futalan, C.-C. Kan, W.-C. Tsai, and M.-W. Wan, "Adsorptive removal of Cu(II) from aqueous solutions using non-crosslinked and crosslinked chitosan-coated bentonite beads," *Desalination*, vol. 275, no. 1–3, pp. 154–159, 2011.

[18] M.-C. Lu, M. L. Agripa, M.-W. Wan, and M. L. P. Dalida, "Removal of oxidized sulfur compounds using different types of activated carbon, aluminum oxide, and chitosan-coated bentonite," *Desalination and Water Treatment*, vol. 52, no. 4–6, pp. 873–879, 2014.

[19] C. V. J. Arida, M. D. G. de Luna, C. M. Futalan, and M.-W. Wan, "Optimization of As(V) removal using chitosan-coated bentonite from groundwater using Box–Behnken design: effects of adsorbent mass, flow rate, and initial concentration," *Desalination and Water Treatment*, vol. 29, pp. 1–9, 2015.

[20] M. J. C. Calagui, D. B. Senoro, C.-C. Kan, J. W. L. Salvacion, C. M. Futalan, and M.-W. Wan, "Adsorption of indium(III) ions from aqueous solution using chitosan-coated bentonite beads," *Journal of Hazardous Materials*, vol. 277, pp. 120–126, 2014.

[21] D. C. Seo, K. Yu, and R. D. DeLaune, "Comparison of monometal and multimetal adsorption in Mississippi River alluvial wetland sediment: Batch and column experiments," *Chemosphere*, vol. 73, no. 11, pp. 1757–1764, 2008.

[22] B. Xiao and K. M. Thomas, "Competitive adsorption of aqueous metal ions on an oxidized nanoporous activated carbon," *Langmuir*, vol. 20, no. 11, pp. 4566–4578, 2004.

[23] L. J. Li, F. Q. Liu, X. S. Jing, P. P. Ling, and A. M. Li, "Displacement mechanism of binary competitive adsorption for aqueous divalent metal ions onto a novel IDA-chelating resin: isotherm and kinetic modeling," *Water Research*, vol. 45, no. 3, pp. 1177–1188, 2011.

[24] E. Malkoc, Y. Nuhoglu, and Y. Abali, "Cr(VI) adsorption by waste acorn of Quercus ithaburensis in fixed beds: Prediction of breakthrough curves," *Chemical Engineering Journal*, vol. 119, no. 1, pp. 61–68, 2006.

[25] L. Cavas, Z. Karabay, H. Alyuruk, H. Doğan, and G. K. Demir, "Thomas and artificial neural network models for the fixed-bed adsorption of methylene blue by a beach waste Posidonia oceanica (L.) dead leaves," *Chemical Engineering Journal*, vol. 171, no. 2, pp. 557–562, 2011.

[26] Q. Yang, Y. Zhong, X. Li et al., "Adsorption-coupled reduction of bromate by Fe(II)–Al(III) layered double hydroxide in fixed-bed column: experimental and breakthrough curves analysis," *Journal of Industrial and Engineering Chemistry*, vol. 28, pp. 54–59, 2015.

[27] C. Y. Yin, M. K. Aroua, and W. M. A. W. Daud, "Fixed-bed adsorption of metal ions from aqueous solution on polyethyleneimine-impregnated palm shell activated carbon," *Chemical Engineering Journal*, vol. 148, no. 1, pp. 8–14, 2009.

[28] A. R. Nesic, S. J. Velickovic, and D. G. Antonovic, "Characterization of chitosan/montmorillonite membranes as adsorbents for Bezactiv Orange V-3R dye," *Journal of Hazardous Materials*, vol. 209-210, pp. 256–263, 2012.

[29] W.-C. Tsai, S. Ibarra-Buscano, C.-C. Kan, C. M. Futalan, M. L. P. Dalida, and M.-W. Wan, "Removal of copper, nickel, lead, and zinc using chitosan-coated montmorillonite beads in single- and multi-metal system," *Desalination and Water Treatment*, vol. 57, pp. 9799–9812, 2016.

[30] V. Brauch and E. U. Schlunder, "The scale-up activated columns for water purification, based on results from batch tests," *Chemical Engineering Science*, vol. 30, pp. 539–548, 1975.

[31] S. Kundu and A. K. Gupta, "As(III) removal from aqueous medium in fixed bed using iron oxide-coated cement (IOCC): experimental and modeling studies," *Chemical Engineering Journal*, vol. 129, no. 1–3, pp. 123–131, 2007.

[32] S. Qaiser, A. R. Saleemi, and M. Umar, "Biosorption of lead from aqueous solution by Ficus religiosa leaves: batch and column study," *Journal of Hazardous Materials*, vol. 166, no. 2-3, pp. 998–1005, 2009.

[33] V. C. Taty-Costodes, H. Fauduet, C. Porte, and Y.-S. Ho, "Removal of lead (II) ions from synthetic and real effluents using immobilized *Pinus sylvestris* sawdust: adsorption on a fixed-bed column," *Journal of Hazardous Materials*, vol. 123, no. 1–3, pp. 135–144, 2005.

[34] O. Hamdaoui, "Dynamic sorption of methylene blue by cedar sawdust and crushed brick in fixed bed columns," *Journal of Hazardous Materials*, vol. 138, no. 2, pp. 293–303, 2006.

[35] H. Nouri and O. Abdelmottaleb, "Modeling of the dynamics adsorption of phenol from an aqueous solution on activated carbon produced from olive stones," *Journal of Chemical Engineering & Process Technology*, vol. 4, no. 3, pp. 1–7, 2013.

[36] B. Volesky and I. Prasetyo, "Cadmium removal in a biosorption column," *Biotechnology and Bioengineering*, vol. 43, no. 11, pp. 1010–1015, 1994.

[37] H. C. Thomas, "Heterogeneous ion exchange in a flowing system," *Journal of the American Chemical Society*, vol. 66, no. 10, pp. 1664–1666, 1944.

[38] G. Yan and T. Viraraghavan, "Heavy metal removal in a biosorption column by immobilized M. rouxii biomass," *Bioresource Technology*, vol. 78, no. 3, pp. 243–249, 2001.

[39] I. Kavianinia, P. G. Plieger, N. G. Kandile, and D. R. K. Harding, "Fixed-bed column studies on a modified chitosan hydrogel for detoxification of aqueous solutions from copper (II)," *Carbohydrate Polymers*, vol. 90, no. 2, pp. 875–886, 2012.

[40] K. H. Chu, "Fixed bed sorption: setting the record straight on the Bohart–Adams and Thomas models," *Journal of Hazardous Materials*, vol. 177, no. 1–3, pp. 1006–1012, 2010.

[41] Young Hee Yoon and J. H. Nelson, "Application of gas adsorption kinetics—II. A theoretical model for respirator cartridge service life and its practical applications," *American Industrial Hygiene Association Journal*, vol. 45, no. 8, pp. 517–524, 1984.

[42] P. Lodeiro, R. Herrero, and M. E. S. D. Vicente, "The use of protonated Sargassum muticum as biosorbent for cadmium removal in a fixed-bed column," *Journal of Hazardous Materials*, vol. 137, no. 1, pp. 244–253, 2006.

[43] Z. Aksu and F. Gönen, "Binary biosorption of phenol and chromium(VI) onto immobilized activated sludge in a packed bed: prediction of kinetic parameters and breakthrough curves," *Separation and Purification Technology*, vol. 49, no. 3, pp. 205–216, 2006.

[44] K. Vijayaraghavan, T. T. Teo, R. Balasubramanian, and U. M. Joshi, "Application of Sargassum biomass to remove heavy metal ions from synthetic multi-metal solutions and urban storm water runoff," *Journal of Hazardous Materials*, vol. 164, no. 2-3, pp. 1019–1023, 2009.